ARTICLE   OPEN

Check for updates

Orbital-optimized pair-correlated electron simulations on trapped-ion quantum computers

Luning Zhao [1✉], Joshua Goings[1], Kyujin Shin [2✉], Woomin Kyoung [2], Johanna I. Fuks [3], June-Koo Kevin Rhee[3,4], Young Min Rhee [5], Kenneth Wright [1], Jason Nguyen[1], Jungsang Kim[1] and Sonika Johri[1]

Variational quantum eigensolvers (VQE) are among the most promising approaches for solving electronic structure problems on near-term quantum computers. A critical challenge for VQE in practice is that one needs to strike a balance between the expressivity of the VQE ansatz versus the number of quantum gates required to implement the ansatz, given the reality of noisy quantum operations on near-term quantum computers. In this work, we consider an orbital-optimized pair-correlated approximation to the unitary coupled cluster with singles and doubles (uCCSD) ansatz and report a highly efficient quantum circuit implementation for trapped-ion architectures. We show that orbital optimization can recover significant additional electron correlation energy without sacrificing efficiency through measurements of low-order reduced density matrices (RDMs). In the dissociation of small molecules, the method gives qualitatively accurate predictions in the strongly-correlated regime when running on noise-free quantum simulators. On IonQ's Harmony and Aria trapped-ion quantum computers, we run end-to-end VQE algorithms with up to 12 qubits and 72 variational parameters—the largest full VQE simulation with a correlated wave function on quantum hardware. We find that even without error mitigation techniques, the predicted relative energies across different molecular geometries are in excellent agreement with noise-free simulators.

INTRODUCTION

Finding accurate solutions to the electronic structure problem is of great importance to various industries, from modeling pharmaceutical drug docking[1], to designing new materials for light harvesting and CO_2 reduction[2], to elucidating reaction mechanisms in novel battery materials[3]. However, the classical computational resources needed to solve the electronic structure problem exactly scales exponentially with the size of systems, which limits routine or practical application to systems with <20 electrons. To make the problem tractable on classical computers, various approximate approaches have been developed, each with different trade-offs between cost and accuracy. These approaches include density functional theory (DFT)[4], coupled cluster (CC)[5] methods, density matrix renormalization group methods (DMRG)[6], and quantum Monte Carlo methods (QMC)[7]. These methods are routinely applied toward computational chemistry calculations both in academia and in industry.

Despite the abundance of different classical approximations, the electronic structure problem is far from being solved. For example, systems with strongly correlated electronic structure are notoriously difficult to solve. These systems are commonly encountered during bond breaking and formation, as well as when studying systems such as transition-metal-containing catalysts, large π-conjugated systems, and high-temperature superconductors. In these cases, approximate approaches may either fail completely (such as in single-reference methods like DFT or CC), or will be prohibitively costly (such as in multi-reference methods like DMRG or QMC). It is possible that approximate classical approaches will never reliably solve the strong correlation problem.

In contrast, quantum computation[8] has attracted significant attention for its potential to solve certain computational problems more efficiently than with classical computers, especially since IBM launched the first cloud accessible quantum computer and Google demonstrated quantum advantage[9]. One of its most promising applications is to solve electronic structure problems efficiently[10]: to illustrate, consider that for a problem containing N spin orbitals, the number of classical bits required to represent the wave function scales combinatorially with N, while on a quantum computer only N qubits are needed. The exponential advantage offered by quantum computers has motivated a great deal of research in developing quantum algorithms to solve the electronic structure problem.

Of these, the variational quantum eigensolver (VQE) algorithm[11–15] is designed specifically for current near-term intermediate scale quantum (NISQ) computers. VQE estimates the ground state of a system by implementing a shallow parameterized circuit, which is classically optimized to variationally minimize the energy expectation value. The VQE algorithm allows the user to select the form of the parameterized circuit. This flexibility allows one to adjust the circuit depth based on the quantum gate fidelity, number of qubits, and desired accuracy. This makes VQE especially suitable for the NISQ era.

There is, however, no free lunch and the ability to run shallower circuits within the VQE comes with two costs. First, the predicted energy in most cases remains approximate, because the accuracy depends on the expressivity of the circuit form. Second, one needs to perform a large number of measurements for VQE. This makes the choice of the ansatz perhaps the most important building block in the VQE algorithm. Early demonstrations of VQE on quantum hardware utilized the physically-motivated unitary

[1]IonQ Inc, College Park, MD 20740, USA. [2]Materials Research & Engineering Center, R&D Division, Hyundai Motor Company, Uiwang 16082, Republic of Korea. [3]Qunova Computing, Daejeon 34051, Republic of Korea. [4]School of Electrical Engineering, KAIST, Daejeon 34141, Republic of Korea. [5]Department of Chemistry, KAIST, Daejeon 34141, Republic of Korea. ✉email: zhao@ionq.co; shinkj@hyundai.com

npj

Table 1. Techniques and their corresponding effects used in the paper.

Technique	Effect	Previous work
Electron Pair → Bosons	Reduce number of qubits by a factor of 2	[15]
Givens Rotation with Magic Gate	Most efficient Givens rotation implementation in terms of CX gates	[50]
Hamiltonian Grouping	3 circuits per energy measurements regardless of system size	[51]
Measurement of RDMs	*3 circuits for all 1- and 2-RDMs regardless of system size*	this work
Orbital Optimization with Newton-Raphson	*Increase circuit expressivity without increasing depth*	this work

coupled cluster with singles and doubles (uCCSD) ansatz[16–18]. uCCSD is well-known in the quantum chemistry community to be able to treat strongly correlated systems, while remaining classically intractable. As such, A. Peruzzo et al.[11] used the uCCSD ansatz in the first VQE demonstration on a photonic quantum computer to solve for the H_2 molecule in a minimal basis. O'Malley et al.[12] performed the same simulations on a superconducting quantum computer with two qubits. In 2018, Hempel[19] et al. simulated H_2 and LiH on a trapped-ion quantum system using $^{40}Ca^+$ ions. In 2019, McCaskey[20] et al. simulated metal hydrides in a 2-electron, 2-orbital active space using the uCCSD ansatz on IBM's superconducting quantum computers with four qubits. However, going beyond a minimal active space poses difficulties due to the rapid increase in the number of entangling gates for the uCCSD ansatz. The number of entangling gates in uCCSD (e.g., $CNOT$) scales as $O(N^4)$, where N is the number of qubits. Even the most efficient implementation of uCCSD circuits contain thousands of entangling gates for small systems[21], which makes it impractical to run on NISQ quantum computers.

Due to the impracticality of the uCCSD ansatz on NISQ quantum computers, hardware efficient ansatzes (HEA)[13,22–25] have attracted significant attention. Compared to the uCCSD ansatz, HEAs need significantly shallower circuits. In 2017, researchers from IBM published the first study[13] of using HEAs on superconducting quantum computers to simulate H_2, LiH, and BeH_2 with 2, 4, and 6 qubits. However, noise in the quantum processing unit (QPU) led to unphysical behavior in the predicted dissociation curve. In 2019, the same researchers[26] use HEAs to demonstrate quantum error mitigation using the zero-noise extrapolation technique with 4 qubits. In 2021, researchers[27] used HEAs to study thermally activated delayed fluorescence (TADF) with 2 qubits on superconducting quantum computers. They found that without using an unscalable error mitigation approach, even a 2-qubit circuit yields qualitatively inaccurate predictions to the relative energy.

The largest VQE simulation performed on quantum hardware so far is the Hartree-Fock (HF) study by Google[14], in which they used a superconducting quantum computer to simulate the HF wave function for hydrogen chains up to 12 qubits and 72 entangling gates. However, the calculations faced a considerable amount of hardware noise, necessitating the use of Hartree-Fock specific error mitigation techniques to achieve sufficiently accurate results, which does not apply for non-HF wave functions. A more recent study by Google[28] simulated a cyclobutene ring on a superconducting quantum computer with up to 10 qubits using pair-correlated wave functions. Here, the ansatz was classically pre-optimized on a simulator, leaving the final energy evaluation to be executed on the quantum device. Despite this, this calculation still required classical error mitigation techniques to achieve reasonable results for the final quantum energy evaluation.

Trapped-ion quantum computers have several advantages over other currently available quantum computing architectures. First, the gate fidelity for trapped-ion qubits is typically higher than for superconducting qubits, which enables users to run deeper circuits. Second, trapped-ion qubits are all-to-all connected. This means one is able to entangle arbitrary pairs of qubits without performing expensive *SWAP* operations to entangle non-adjacent qubits, which is usually required on systems with interactions that do not form a complete graph. Although both of these advantages should lead to higher fidelity when running VQE circuits, implementations of VQE on trapped-ion quantum computers are rare, and this is mainly due to comparatively limited availability of the trapped-ion quantum computing hardware versus superconducting quantum computers. In this work, we fill this gap by performing VQE simulations on two generations of trapped-ion quantum computers constructed by IonQ, Inc.

We consider an approximate ansatz derived from the uCCSD ansatz: the unitary pair CCD (upCCD) ansatz, in which only paired double excitations are retained. This allows us to map the fermionic representation to electron pairs, known as the hard-core boson representation. From this, we show that the unitary pCCD ansatz then requires half the number of qubits to encode the state vector as compared to the uCCSD ansatz. We then introduce the optimal circuit for implementing an arbitrary electron pair excitation in terms of the number of CX gates. The energy expression for the upCCD ansatz is derived, and we find that at most 3 circuits are needed to compute the energy expectation value, regardless of the size of the system. The shallow circuit structure, along with a constant low number of measurements required, make the upCCD ansatz a perfect candidate on NISQ quantum computers.

The accuracy of the upCCD ansatz depends on the choice of the underlying orbitals. Previous studies on similar wave functions have found that it is necessary to optimize the orbitals along with the cluster amplitudes, especially for strongly correlated systems. In this work, we find that the orbital optimization effects can be incorporated through classical post-processing, and only requires the measurements of one- and two-body reduced density matrices (RDM) of the upCCD ansatz on the quantum device. In our experiments, we observe that failure to use orbital optimization results in highly non-physical energy predictions in the bond-dissociation regime, but physical behavior can be fully recovered by optimizing orbitals together with parameters in the upCCD ansatz. Due to the symmetry of the upCCD ansatz, the energy measurements automatically yield the required measurements for RDMs. This allows us to improve the expressivity of the ansatz, especially for strongly correlated systems without increasing the circuit depth on the quantum computer. In Table 1, we list a collection of techniques used in the study, with inventions in this work marked in *italic*. Our result (see Table 2) is the largest full VQE demonstration on a QPU using a correlated wave function.

The paper is structured as follows. We begin by introducing the upCCD ansatz, then discuss the mapping from electron pairs to Pauli matrices, and an efficient quantum circuit implementation of the ansatz. We then derive the energy expression for the upCCD ansatz. Having laid out the general formalism, we then introduce the orbital optimization of upCCD using RDMs and the Newton-Raphson algorithm. Results are presented on quantum simulators and IonQ's Harmony and Aria quantum computers for potential energy surface predictions of LiH, H_2O, and Li_2O molecule. All the VQE experiments on simulator and quantum computers are end-

npj

Table 2. Comparison between this work and previous publicly-reported VQE chemistry simulations on QPUs.

Year	Ansatz	System	# Qubits	# Parameters	2QGE[a]	Full VQE?	Error Mitigation?	Hardware Vendor
2022	oo-upCCD [this work]	Li_2O	12	72	12	Yes	Yes	IonQ
2022	upCCD[28]	Cyclobutene Ring	10	25	25	No	Yes	Google
2022	uCCSD[52]	CH_3	6	4	7	No	Yes	Quantinuum
2022	YXXX[53]	oxazine derivatives	4	1	N/A[b]	Yes (superconducting), No (trapped-ion)	Yes	IBM, Quantinuum
2022	uCCSD-PBC[54]	crystalline iron model	2	1	2	Yes	Yes	IBM
2022	Entang. Forging[55]	H_3S^+	6	8	19	No	Yes	IBM
2022	Entang. Forging[56]	H_2O	5	3	11	Yes	Yes	IBM
2021	HEA[3]	LiH (dipole moment)	4	16	9	Yes	Yes	IBM
2021	HEA[27]	TADF	2	4	1	Yes	Yes	IBM
2021	qubit CC[34]	H_{10}	2	3	1	No	Yes	IonQ
2021	HEA[57]	Li_2O_4 model	2	4	1	Yes	Yes	IBM
2020	Hartree-Fock[14]	H_{12}	12	36	72	Yes	Yes	Google
2020	upCCD[15]	H_2O	3	3	6	Yes	No	IonQ
2019	HEA[26]	LiH	4	20	9	Yes	Yes	IBM
2019	reduced uCC[20]	NaH, KH, RbH	4	3	8	No	Yes	IBM, Rigetti
2018	uCCSD[19]	LiH	3	2	4	Yes	No	UInn
2018	uCCSD[44]	H_2 (excited states)	2	1	1	Yes	No	UCB, LBNL
2017	HEA[13]	BeH_2	6	30	5	Yes	No	IBM
2016	uCCSD[12]	H_2	2	1	2	No (scan)	No	UCSB
2014	uCCSD[11]	HeH^+	2	6	1	Yes	No	Univ. of Bristol

[a]2QGE: 2-qubit gate equivalents.
[b]The authors did not provide this in their paper.

to-end VQE runs, which means we perform both parameter optimizations and final energy evaluations. We conclude with a summary of our findings and comments on future directions.

Readers are strongly encouraged to read "Methods" section before "Results" section. In "Methods" section, we describe the details of the quantum computer hardware used to run VQE and the specifics of the molecular models used to generate the quantum simulation circuits. We heavily use the notations defined in "Methods" section throughout "Results" section.

RESULTS
The VQE algorithm and circuit
The unitary pair Coupled Cluster double (upCCD) ansatz is

$$\left|\Psi_{upCCD}\right\rangle = e^{T-T^\dagger}\left|HF\right\rangle \qquad (1)$$

in which T is the pair-double cluster operator, defined as

$$T = \sum_{ia} t_i^a a_{a\alpha}^\dagger a_{a\beta}^\dagger a_{i\beta} a_{i\alpha} \qquad (2)$$

in which i and a are indices for occupied and unoccupied orbitals in the HF state. $a_{p\alpha}^\dagger$ ($a_{p\beta}^\dagger$) and $a_{p\alpha}$ ($a_{p\beta}$) are the Fermionic creation and annihilation operators in the pth spin up (down) orbital.

Each exponentiation of the pair-excitation operator can be efficiently implemented with the following circuit in Fig. 1,

Once the circuit is defined, one needs to measure the energy expectation value $\langle\Psi_{upCCD}|H|\Psi_{upCCD}\rangle$ for the second-quantized Hamiltonian H. Originally, there are $O(N^4)$ terms in H, in which N is the number of qubits. However, a majority of them do not
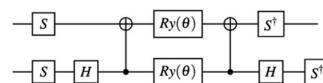
Fig. 1 A quantum circuit that implements the Givens rotation. S and $S^\dagger$ are the phase gate and its inverse. H is the Hadamard gate. $R_y(\theta)$ is the single qubit rotation gate by angle θ around the axis. Entangling gates are CNOT gates.

contribute to the energy since they break pair symmetry. After eliminating these terms, one finds that only 3 measurements are needed in the X, Y, and Z basis respectively to compute the energy, regardless of the system size.

The upCCD ansatz defined in Eq. (1) is not invariant to the choice of underlying orbitals. Previous studies[29-32] on similar wave functions have found that it is necessary to optimize the orbitals along with the cluster amplitudes, especially for strongly correlated systems. The orbital optimized upCCD ansatz is

$$\left|\Psi_{oo-upCCD}\right\rangle = e^K e^{T-T^\dagger}\left|HF\right\rangle \qquad (3)$$

in which there are two different sets of parameters: (1) circuit parameters in the cluster operator T; (2) orbital rotation parameters in the the orbital rotation operator K, which is defined as

$$K = \sum_{p>q}\sum_\sigma K_{pq}(a_{p\sigma}^\dagger a_{q\sigma} - a_{q\sigma}^\dagger a_{p\sigma}) \qquad (4)$$

where K is an anti-Hermitian matrix and σ indexes the spin.
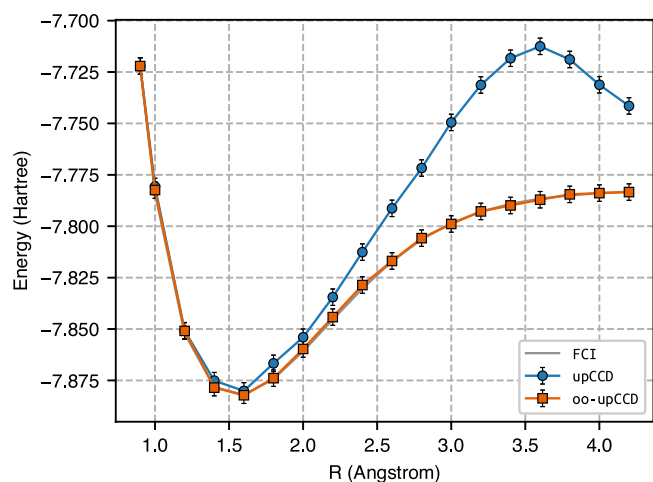
Fig. 2 Dissociation of LiH in STO-3G basis set comparing upCCD, oo-upCCD, and FCI. VQE results are obtained from a noise-free quantum simulator. The error bars correspond to finite sampling error of $\pm 1\sigma$.

Fig. 3 Dissociation of LiH in STO-3G basis set comparing oo-upCCD VQE results obtained from the IonQ Harmony and Aria quantum computer and FCI. The error bars correspond to finite sampling error of $\pm 1\sigma$.

As shown in the Methods section, we find the optimal set of orbital rotation parameters K_{pq} with the Newton-Raphson (NR) algorithm, in which the energy gradient and Hessian are measured on the quantum computer. Then, the effect of orbital rotation operators can be fully absorbed into one- and two-electron integrals through integral transformation, which is done efficiently on classical computers. Therefore, although doing orbital optimization increase the number of variational parameters significantly, it does not increases the complexity of the quantum experiments since both the circuit depth and the number of measurements remain the same. However, it has been shown before[29] that optimizing these parameters is not a trivial task for classical optimizers, so that measuring them accurately on the the quantum computer will be crucial for a successful optimization.

Experimental examples

All the calculations and experiments were performed using IonQ's in-house quantum chemistry library, which facilitates the preparation and execution of quantum variational algorithms on IonQ's cloud simulators and QPUs. We used the PySCF[33] software suite to compute the molecular integrals necessary to define the second-quantized Hamiltonian, as well as compute the classical FCI reference energies.

We begin with our bond dissociation results with a simple example, the LiH molecule. The system has only two valence electrons. We freeze the Li $1s$ orbital, and also exclude the molecular orbitals formed with Li's $2p_x$ and $2p_y$ orbitals since they do not contribute to the correlation energy due to symmetry. By doing so we only need 3 qubits and the VQE circuits consists of only 4 CX gates. In Fig. 2, we compare the energy predicted by FCI, upCCD, and oo-upCCD. As shown in the plot, both upCCD and oo-upCCD provide accurate energy predictions for the molecule when the bond distance is less than or equal to the equilibrium bond length (1.6 Angstrom). We refer to these as "squeezed" and "equilibrium" geometries. On the other hand, when we begin to extend the Li-H bond beyond the equilibrium bond length, what we refer to as the "stretched" geometry, the energy error not only increases to tens of millihartrees, but it also exhibits a "hump" in the potential energy surface (PES). Such a non-physical behavior is primarily due to the break down of the mean-field picture in bond breaking scenarios. To the contrary, the oo-upCCD energy prediction matches FCI in both equilibrium and the stretched regions, which demonstrates the importance of orbital optimization.
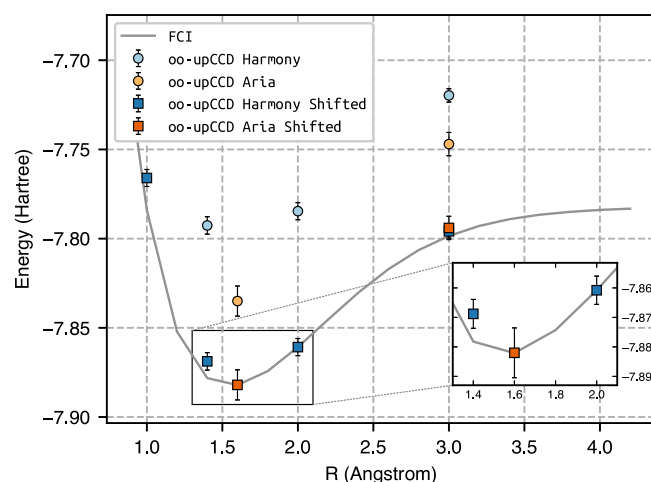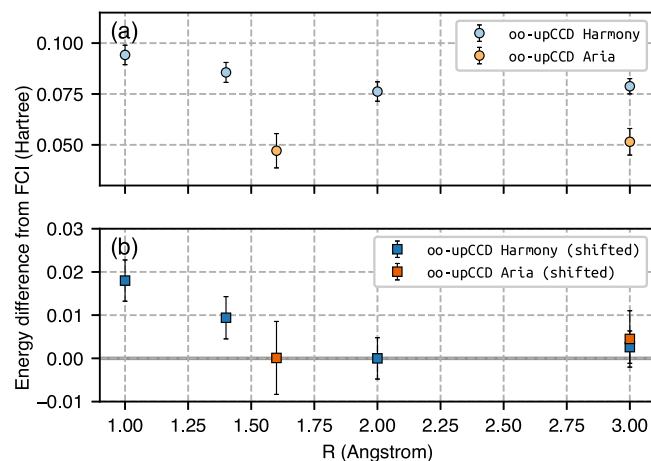
Fig. 4 Energy difference with respect to FCI for the dissociation of LiH in STO-3G basis set. The top (**a**) shows the raw energy difference from FCI, while the bottom (**b**) shows the energy difference from FCI when shifted by an empirical constant scalar. VQE results are obtained from the IonQ Harmony and the IonQ Aria quantum computer. The error bars correspond to finite sampling error of $\pm 1\sigma$.

We then move from simulators to quantum hardware. In Figs. 3 and 4, we show the results obtained from IonQ's Harmony quantum computer. The system has 11 all-to-all connected qubits, and the averaged single and two-qubit gate fidelities are 99% and 98%. It has been used in numerous applications, including quantum chemistry[15,34], quantum machine learning[35,36], and finance[37,38]. Due to the limited machine time, instead of scanning the entire PES, we selected a few points from squeezed, equilibrium, and stretched geometries. As shown in the plot, the energy measured on noisy quantum hardware is much higher than the simulation results. However, we also find that the amount of error is consistent along the PES. Based on such an observation, we shifted all the measured energies by a constant (-0.0762 Hartree). By doing so, the shifted energies matches well with the exact energy. This is notable especially with the stretched geometry $R = 3.0$ Angstrom, in which the shifted energy falls on the simulated PES of oo-upCCD, demonstrating that the orbital optimization effects are successfully captured by the quantum

hardware. Although the shifted energies can be considered a form of error mitigation, we note that the exact shift requires the availability of noiseless simulation results, which is generally not the case for circuits that are not classically simulatable. Therefore, one should think of the shift as merely a way to demonstrate that the relative energies—which are of more utility in practice—are still accurate despite the presence of noise.

Lastly, we ran the same simulation on IonQ Aria: IonQ's latest generation quantum computer and the results are shown in Figs. 3 and 4. IonQ Aria offers both more qubits and improved gate fidelities over IonQ Harmony. We find that the improved gate fidelities reduces the amount of error in energy by 38%. Once shifted (by -0.047 Hartree), the relative energy also matches the exact energy within statistical uncertainty. The improvements from Harmony to Aria are not very large in this case due to the simplicity of the circuit, which contains only 4 CX gates. For the LiH calculations conducted on Harmony and Aria, the average deviations from the ideal oo-pUCCD simulations are found to be 7.6 ± 4.6 millihartrees for Harmony, and 2.6 ± 7.5 millihartrees for Aria.

Our next example is the symmetric double dissociation of H_2O, as shown in Supplementary Fig. 4 for results obtained on the simulator. We only freeze the O 1s core orbital and keep all other orbitals in the active space. The total number of qubits required is 6 and there are 16 CX gates in the circuit. Again, oo-upCCD produces highly accurate energies compared with FCI. However, unlike LiH, in which oo-upCCD matches FCI exactly, in H_2O we find the predicted energy error for oo-upCCD is about 20 millihartrees, especially when we are in the stretched geometry. The error is due to the omission of the un-paired excitations in the oo-upCCD ansatz. However, we also note that without orbital optimization, the upCCD ansatz using the HF orbitals yields more than 200 millihartrees of error in energy, again emphasizing the importance of orbital optimization. For the H_2O calculations conducted on Aria, the average deviation from the ideal oo-pUCCD simulations is found to be 5.6 ± 10.8 millihartrees.

Before running the circuit on quantum hardware, we first remove redundant parameters from the ansatz. The redundant parameters are the circuit parameters that do not contribute to the energy, and their amplitudes stay zero during the optimization process. For the H_2O molecule, an example of redundant parameters are the amplitudes that correspond to pair excitations from the non-bonding orbital. In this study, we identify redundant parameters by tracking the evolutions of parameter amplitudes on a noise-free simulator, with all parameters started from zero. Parameters whose amplitudes stay at zero during the entire optimization process are identified as redundant parameters. It is worth noting that such an approach does not scale as the system size, and the running time on simulator becomes prohibitively expensive. Fortunately, there exist scalable approaches for identifying and simulating only non-redundant parameters, such as the gradient based selection used for the ADAPT-VQE[17] method.

Upon removal of redundant parameters, we are able to reduce the circuit to contain 4 circuit parameters and 8 CX gates. We then performed the oo-upCCD simulation on IonQ's Aria quantum computer, and the results are shown in Fig. 5. The simulation is done on two geometry points: one at the equilibrium geometry and the other one at the stretched geometry. We find that the Aria quantum computer successfully finds the optimal parameters and captures the orbital optimization effects. Similar to LiH, the noise on the hardware introduce a systematic, positive bias to the measured absolute energy, but such a bias is constant at different geometry points. Once we shift the absolute energies by a constant, the energies match the ones measured on a noise-free simulator, which demonstrates that the hardware noise is consistent enough so that the predicted relative energies are accurate.
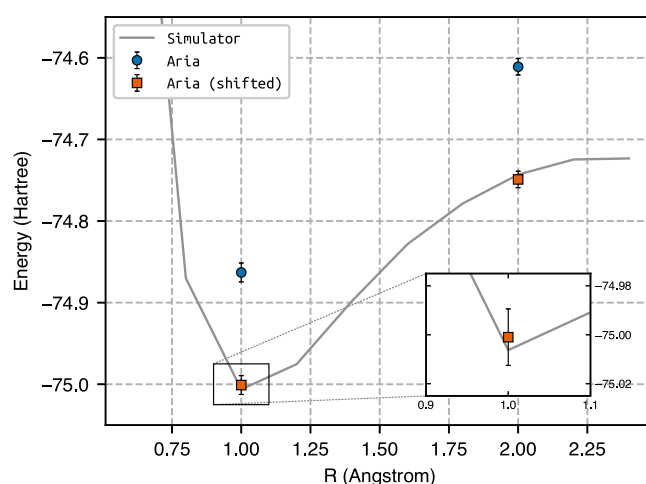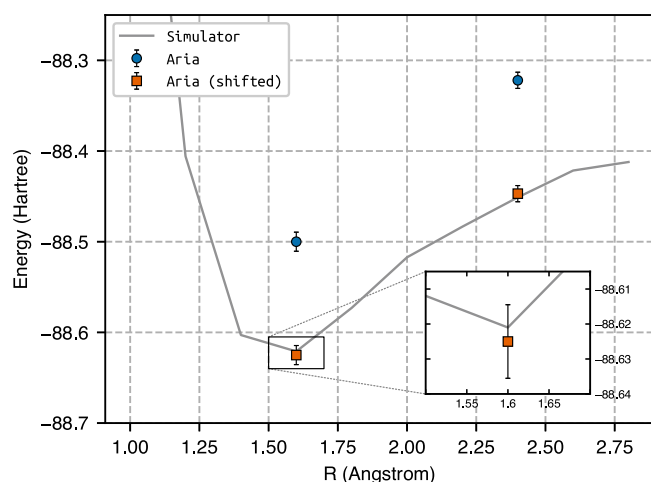

Fig. 5 Dissociation of H_2O in STO-3G basis set comparing oo-upCCD VQE results obtained from the IonQ Aria quantum computer and a noise-free simulator. The error bars correspond to finite sampling error of $\pm 1\sigma$.

Our final example is the symmetric dissociation of the Li_2O molecule. Li_2O is one of the secondary reaction products in lithium-air batteries, which is believed to be a candidate for next-generation lithium battery due to its high energy density. We freeze the 1s orbital for Li and O, resulting in a circuit with 12 qubits and 64 CX gates. The results on an ideal simulator are shown in Supplementary Fig. 5. The difference in energy between oo-upCCD and FCI becomes more noticeable than in LiH and H_2O. Such a difference is expected since the size of the Hilbert of Li_2O is much larger than that of LiH and H_2O, which means that there are a lot more electronic configurations that break electron pairs in Li_2O, and these configurations will contribute to the correlation energy. Due to the pair-approximation made by oo-upCCD, these configurations are neglected, which then leads to a much larger amount of error v.s. FCI. Again, we find that orbital optimization does not make any noticeable amount of difference in equilibrium geometry, but becomes crucial in stretched geometries.

We then performed the oo-upCCD simulation on the Aria quantum computer. Analogous to H_2O, we first identify and remove redundant parameters. In this example we find that only 6 out of the 32 circuit parameters are non-redundant. Therefore, we only implement and optimize these 6 circuit parameters (12 CX gates) on the quantum hardware, with an additional 66 orbital rotation parameters, for 72 variational parameters total. The results are shown in Fig. 6 at two geometry points: one at the equilibrium geometry and another one at the stretched geometry. For the Li_2O calculations conducted on Aria, the average deviation from the ideal oo-pUCCD simulations is found to be 4.0 ± 9.7 millihartrees. Similar to the case of H_2O, we find that despite hardware noise, the predicted relative energy matches the simulator's prediction, and the orbital optimization effects are successfully captured by Aria.

DISCUSSION
Quantum computers are expected to be able to efficiently solve the electronic structure problem. In principle, the electronic energy can be exactly computed in polynomial time using quantum phase estimation (QPE)[39] or its iterative variant[40]. In contrast, the best equivalent classical algorithm (full configuration interaction, or FCI) scales exponentially. In QPE, one implements the time propagator $U = \exp(-iHt)$ on the quantum computer and operates it on an efficiently prepared trial state. Assuming the

Fig. 6 Dissociation of Li₂O in STO-3G basis set comparing oo-upCCD VQE results obtained from the IonQ Aria quantum computer and a noise-free simulator. The error bars correspond to finite sampling error of $\pm 1\sigma$.

trial state has sufficient overlap with the exact eigenstate $|\Psi_i\rangle$, the exact eigenstate's energy is encoded in the phase of the wave function since $U|\Psi_i\rangle = \exp(-iE_i t)|\Psi_i\rangle$. The phase can be extracted using the quantum Fourier transform (QFT).

While the QPE algorithm can compute the energy levels of molecules exactly, it is impractical on current NISQ computers. In the NISQ era, quantum gates are noisy, and entangling gates are typically an order of magnitude lower in fidelity compared to single qubit gates. This means that one can only perform a limited number of quantum operations to ensure that the results are distinguishable from noise. This poses a significant difficulty for the QPE algorithm, as the implementation of the time propagator is very expensive and yields deep quantum circuits. QPE algorithms without using the time propagator, such as qubitization[41–43] have also been developed with improved scaling, but the fact remains that neither algorithm results in circuits that are shallow enough to run on quantum computers without error-corrected qubits.

We therefore focus on VQE, an algorithm expressly designed for NISQ computers. Here, we have developed an efficient VQE algorithm that is able to run on near-term quantum computers with high accuracy. The algorithm employs a chemically-inspired ansatz based on the unitary pair coupled cluster doubles (upCCD) wave function. The upCCD ansatz is obtained from the general unitary-CCSD ansatz by retaining only paired double excitations. This allows us to condense electron pairs to the hard-core boson representation and develop an efficient quantum circuit implementation that only requires 2 *CX* gates to implement one excitation. Since the accuracy of the upCCD ansatz depends on the underlying orbital choice, we developed an orbital optimization algorithm that finds the variationally optimal set of orbitals automatically. We find that orbital optimization can be implemented efficiently by measuring one- and two-body RDMs on a quantum computer and computing integral transformations on a classical computer.

We tested the oo-upCCD VQE approach on the bond dissociation pathways for LiH, H₂O, and Li₂O molecule on both quantum simulators and IonQ's Harmony and Aria quantum computers. We find that on quantum simulators, oo-upCCD gives qualitatively accurate predictions to energy both in the weakly correlated and strongly correlated regime. However, upCCD without orbital optimization produces unphysical behavior in the strongly correlated regime. On quantum hardware, we observed that noisy quantum gate operations yield a consistent

positive bias for the energy. Such a consistent bias has also been observed before[28]. In order to understand this, we have performed simulations with both coherent and incoherent noise models on quantum simulators. We find that if the error rate is low enough (below 1%), both error models produce a constant additive error for different molecular geometries, which aligns with the error rate of the Harmony and Aria quantum computers. The simulation results can be found in the Supplementary Note 8. Therefore, although the measured absolute energies can be higher than simulator results by hundreds of millihartrees, the relative energies measured are accurate due to the consistency of errors across the PES (i.e., low non-parallelity error).

As with other seniority zero approaches, oo-upCCD proves effective for describing some strong electron correlations but is unable to deliver quantitative accuracy, a difficulty that may in future be addressed in two different ways. First, one may consider implementing the full unitary-CCSD ansatz with quantum circuits, and pay the price of ending up with very deep circuits that are not practical to run on NISQ devices, even with the most efficient compilation techniques. A more practical way is to trade-off circuit depths with measurements and employ approaches such as the quantum subspace expansion (QSE)[44,45]. QSE will be able to solve two problems at the same time: (1) account for correlations contributed from non-bosonic excitations. and (2) account for correlations contributed from orbitals that are outside of the active space. QSE is able to achieve these two goals without increasing circuit depth, by just performing more measurements to compute higher order RDMs.

In order to achieve quantitative accuracy on a noisy quantum computer using VQE, one would inevitably perform some form of error mitigation. Over the past few years, various error mitigation methods have been developed, such as noise extrapolation[26], density matrix purification[14,20], symmetry verification[46], randomized compiling[47], and noise-estimation[48]. We believe that an efficient VQE approach combined with measurement based post-processing and noise estimation is a very promising route that harvests the most performance out of near-term quantum computers. Together with continued improvements in quantum hardware, both in terms of qubit number and qubit quality, we will soon see quantum simulation of molecules and materials that surpasses the best classical supercomputers.

METHODS

Trapped-Ion quantum computer

The experimental demonstration was performed on two generations of quantum processing units (QPU) from IonQ: Harmony and Aria. Both QPUs utilize trapped Ytterbium ions where two states in the ground hyperfine manifold are used as qubit states. These states are manipulated by illuminating individual ions with pulses of 355 nm light that drive Raman transitions between the ground states defining the qubit. By configuring these pulses, arbitrary single qubit gates and Mølmer-Sørenson type two-qubit gates can both be realized. The IonQ Aria QPU features not only an order of magnitude better performance in terms of fidelity but also is considerably more robust compared to the IonQ Harmony QPU[49].

upCCD circuit design

From the electron pair excitation operators, we can define the pair creation and annihilation operators

$$d_a^\dagger = a_{a\alpha}^\dagger a_{a\beta}^\dagger$$
$$d_i = a_{i\beta} a_{i\alpha}$$

(5)

in which a_i and $a_i^\dagger$ are the fermionic annihilation and creation operators on orbital i. α and β indicate spin up and spin down.

They follow bosonic symmetries

$$[d_a^\dagger, d_i] = 0$$
$$[d_i, d_j] = [d_a^\dagger, d_b^\dagger] = 0 \tag{6}$$

By performing the Jordan-Wigner Transformation (JWT) to map molecular orbitals to qubits, the pair creation and annihilation operators becomes

$$d_a^\dagger \rightarrow \frac{1}{2}(X_a - iY_a)$$
$$d_i \rightarrow \frac{1}{2}(X_i + iY_i) \tag{7}$$

The pair-excitation operator becomes

$$d_a^\dagger d_i \rightarrow \frac{1}{4}(X_a X_i + iX_a Y_i - iY_a X_i + Y_a Y_i) \tag{8}$$

As one can see from the above equation, after JWT, the pair excitation operator does not have the Pauli-Z strings that occur in general double excitations, due to its bosonic nature.

The exponential of the pair-excitation operator, subtracted by its complex conjugate, becomes

$$\exp\left(t_i^a(d_a^\dagger d_i - d_i^\dagger d_a)\right) = \exp\left(\frac{it_i^a}{2}(X_a Y_i - Y_a X_i)\right). \tag{9}$$

One can then show that this is the Givens rotation matrix

$$\begin{pmatrix} 1 & 0 & 0 & 0 \\ 0 & \cos\left(\frac{t_i^a}{2}\right) & -\sin\left(\frac{t_i^a}{2}\right) & 0 \\ 0 & \sin\left(\frac{t_i^a}{2}\right) & \cos\left(\frac{t_i^a}{2}\right) & 0 \\ 0 & 0 & 0 & 1 \end{pmatrix} \tag{10}$$

As has been shown before[50], the Givens rotation matrix belongs to the **SO**(4) group, which can be implemented in 12 elementary (i.e., R_y, R_z) gates and 2 CX gates using the magic gate basis shown in Fig. 7.

The efficient Givens rotation implementation with angle θ is then given at Fig. 1, in which only two CX gates are required.

Hamiltonian and energy measurements

Since the upCCD ansatz conserves electron pairs, the terms in the ab initio Hamiltonian that break electron pairs do not contribute to energy. After removing these terms, the Hamiltonian can be written as

$$H = H_1(n_p) + H_2(d_p^\dagger d_q) \tag{11}$$

in which the first term only depends on the number operator

$$n_p = a_p^\dagger a_p \rightarrow \frac{1}{2}(1 - Z_p), \tag{12}$$

and so it can be measured in the computational basis.

The second term only depends on the pair excitation operator defined in Eq. (8). Furthermore, we note that the two middle terms in it are associated with purely imaginary coefficients, which do not contribute to energy, so that this term can be measured with all qubits in either the X or Y basis. In summary, only 3 circuits are needed to be run in order to measure the energy expectation value for the upCCD ansatz, compared with a number of measurements that scales as $O(N^4)$ (where N is the number of
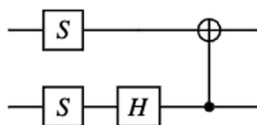
Fig. 7 A quantum circuit that implements the transformation to the Magic gate basis. S and S^dagger are the phase gate and its inverse. H is the Hadamard gate. *CNOT* Entangling gatesare gates.

orbitals) if no symmetry is exploited, independent of the size of the system. This makes the upCCD ansatz extremely efficient in terms of number of measurements.

Orbital optimization based on measurements

The orbital optimization effects can be performed classically with integral transformation. Consider the energy expectation value of the oo-upCCD ansatz.

$$E = \langle\Psi_{\text{upCCD}}|e^{-K}He^K|\Psi_{\text{upCCD}}\rangle \tag{13}$$

where K is an anti-Hermitian operator defined in Eq. (4). We first organize the elements of the lower triangle of K into the length-d vector $\boldsymbol{\kappa}$, where

$$d = (n_o + n_v)(n_o + n_v - 1)/2 \tag{14}$$

Starting from initial orbitals ($\boldsymbol{\kappa} = 0$), we expand the energy out to second order in $\boldsymbol{\kappa}$ to obtain

$$E(\boldsymbol{\kappa}) \approx E(0) + \boldsymbol{\kappa}^T\boldsymbol{\omega} + \frac{1}{2}\boldsymbol{\kappa}^T Q\boldsymbol{\kappa} \tag{15}$$

where the length-d energy gradient $\boldsymbol{\omega}$ and the $d \times d$ energy Hessian Q are given by

$$\omega_x = \frac{\partial E(\boldsymbol{\kappa})}{\partial \kappa_x}$$
$$Q_{xy} = \frac{\partial^2 E(\boldsymbol{\kappa})}{\partial \kappa_x \partial \kappa_y} \tag{16}$$

which in turn are functions of the spinless one- and two-electron reduced density matrices (RDM)

$$\gamma_{pq} = \langle\Psi|a_{p\alpha}^\dagger a_{q\alpha} + a_{p\beta}^\dagger a_{q\beta}|\Psi\rangle$$
$$\Gamma_{pr}^{qs} = \langle\Psi|\frac{1}{2}a_{p\alpha}^\dagger a_{q\alpha} a_{r\alpha}^\dagger a_{s\alpha} + \frac{1}{2}a_{p\beta}^\dagger a_{q\beta} a_{r\beta}^\dagger a_{s\beta} + a_{p\alpha}^\dagger a_{q\alpha} a_{r\beta}^\dagger a_{s\beta}|\Psi\rangle \tag{17}$$

Since the spinless RDMs are in the form of expectation values, they can be measured on the quantum computer, and since we only need 1- and 2-RDMs, the cost for measuring them is the same as measuring the energy. Using $\boldsymbol{\omega}$ and Q, we can choose a $\boldsymbol{\kappa}$ that reduces the energy using the Newton-Raphson (NR) method,

$$\boldsymbol{\kappa} = -Q^{-1}\boldsymbol{\omega} \tag{18}$$

At this point, $\boldsymbol{\kappa}$ becomes nonzero, and the energy expectation value of the oo-upCCD ansatz is written in Eq. (13). There are two ways to compute it. The first one is to implement $e^K|\Psi_{\text{upCCD}}\rangle$ with a quantum circuit. However, one could see that doing so would dramatically increase the circuit depth due to the additional unitary operator e^K. The second way is what we take in this study. Instead of implementing $e^K|\Psi_{\text{upCCD}}\rangle$, we first compute

$$\tilde{H} = e^{-K}He^K \tag{19}$$

since K is anti-Hermitian only contains one-body operators, such a transformation could be computed efficiently on classical computers through standard integral transformation. The detailed expression of $\tilde{H}$ could be found in the Supplementary Note 4.

With $\tilde{H}$, the energy expectation value becomes $\langle\Psi_{\text{upCCD}}|\tilde{H}|\Psi_{\text{upCCD}}\rangle$. As one could see, now $\boldsymbol{\kappa}$ becomes zero again since its effects have been absorbed into the Hamiltonian. At this point, another NR step can be taken, and the method can be iterated to convergence. In this way, since $\boldsymbol{\kappa}$ is always zero, we do not need to implement it with quantum circuits. The VQE algorithm is shown in Algorithm 1, and the detailed expressions for the orbital gradients and Hessians in terms of 1- and 2-RDMs, as well as an example of VQE convergence with respect to optimization iterations, can be found in the Supplementary Note 4 and 7.

Algorithm 1. VQE Algorithm for oo-upCCD

---

while *Energy not converged* **do**

    Optimize T using SPSA

    Update circuit parameters based on the optimal T^*

    Optimize K using NR

    Update orbital parameters based on the optimal K^*

    Rotate one- and two-electron integrals to the new orbital
     basis

    Set K to be 0

    Compute energy to check convergence

end

DATA AVAILABILITY

The data presented in this paper are available from the corresponding author upon reasonable request.

CODE AVAILABILITY

The software implementation used to perform VQE simulations is not publicly available.

REFERENCES

1. Blunt, N. S. et al. A Perspective on the Current State-of-the-Art of Quantum Computing for Drug Discovery Applications. *J. Chem. Theory Comput.* **18**, 7001–7023 (2022).
2. von Burg, V. et al. Quantum Computing Enhanced Computational Catalysis. *Phys. Rev. Res.* **3**, 033055 (2021).
3. Rice, J. E. et al. Quantum Computation of Dominant Products in Lithium-Sulfur Batteries. *J. Comp. Phys.* **154**, 134115 (2021).
4. Parr, R. G. & Yang, W. *Density-Functional Theory of Atoms and Molecules* (Oxford University Press, New York, 1989).
5. Szabo, A. & Ostlund, N. S. *Modern Quantum Chemistry: Introduction to Advanced Electronic Structure Theory* (Dover Publications, Mineola, N.Y., 1996).
6. Schollwöck, U. The Density-Matrix Renormalization Group. *Rev. Mod. Phys.* **77**, 259–315 (2005).
7. Kent, P. R. C. et al. QMCPACK: Advances in the Development, Efficiency, and Application of Auxiliary Field and Real-Space Variational and Diffusion Quantum Monte Carlo. *J. Comp. Phys.* **152**, 174105 (2020).
8. Nielsen, M. A. & Chuang, I. L. *Quantum Computation and Quantum Information* (Cambridge University Press, Cambridge, 2010).
9. Arute, F. et al. Quantum Supremacy Using a Programmable Superconducting Processor. *Nature* **574**, 505 (2019).
10. Cao, Y. et al. Quantum Chemistry in the Age of Quantum Computing. *Chem. Rev.* **119**, 10856–10915 (2019).
11. Peruzzo, A. et al. A Variational Eigenvalue Solver on a Photonic Quantum Processor. *Nat. Commun.* **5**, 4213 (2014).
12. O'Malley, P. J. J. et al. Scalable Quantum Simulation of Molecular Energies. *Phys. Rev. X* **6**, 031007 (2016).
13. Kandala, A. et al. Hardware-Efficient Variational Quantum Eigensolver for Small Molecules and Quantum Magnets. *Nature* **549**, 242–246 (2017).
14. Google AI Quantum and Collaborators. Hartree-Fock on a Superconducting Qubit Quantum Computer. *Science* **369**, 1084–1089 (2020).
15. Nam, Y. et al. Ground-State Energy Estimation of the Water Molecule on a Trapped-Ion Quantum Computer. *npj Quant. Inf.* **6**, 33 (2020).
16. Grimsley, H. R., Claudino, D., Economou, S. E., Barnes, E. & Mayhall, N. J. Is the Trotterized UCCSD Ansatz Chemically Well-Defined? *J. Chem. Theory Comput.* **16**, 1–6 (2020).
17. Grimsley, H. R., Economou, S. E., Barnes, E. & Mayhall, N. J. An Adaptive Variational Algorithm for Exact Molecular Simulations on a Quantum Computer. *Nat. Commun.* **10**, 3007 (2019).
18. Lee, J., Huggins, W. J., Head-Gordon, M. & Whaley, K. B. Generalized Unitary Coupled Cluster Wave Functions for Quantum Computation. *J. Chem. Theory Comput.* **15**, 311–324 (2019).
19. Hempel, C. et al. Quantum Chemistry Calculations on a Trapped-Ion Quantum Computer. *Phys. Rev. X* **8**, 031022 (2018).
20. McCaskey, A. J. et al. Quantum Chemistry as a Benchmark for Near-Term Quantum Computers. *npj Quant. Inf.* **5**, 99 (2019).
21. Cowtan, A., Simmons, W. & Duncan, R. A Generic Compilation Strategy for the Unitary Coupled Cluster Ansatz. Preprint at https://doi.org/10.48550/arXiv.2007.10515 (2020).
22. Barkoutsos, P. K. et al. Quantum Algorithms for Electronic Structure Calculations: Particle-Hole Hamiltonian and Optimized Wave-Function Expansions. *Phys. Rev. A* **98**, 022322 (2018).
23. Ryabinkin, I. G., Yen, T.-C., Genin, S. N. & Izmaylov, A. F. Qubit Coupled Cluster Method: A Systematic Approach to Quantum Chemistry on a Quantum Computer. *J. Chem. Theory Comput.* **14**, 6317–6326 (2018).
24. Ryabinkin, I. G., Lang, R. A., Genin, S. N. & Izmaylov, A. F. Iterative Qubit Coupled Cluster Approach with Efficient Screening of Generators. *J. Chem. Theory Comput.* **16**, 1055–1063 (2020).
25. Anselmetti, G.-L. R., Wierichs, D., Gogolin, C. & Parrish, R. M. Local, Expressive, Quantum-Number-Preserving VQE ansätze for Fermionic Systems. *New J. Phys.* **23**, 113010 (2021).
26. Kandala, A. et al. Error Mitigation Extends the Computational Reach of a Noisy Quantum Processor. *Nature* **567**, 491–495 (2019).
27. Gao, Q. et al. Applications of Quantum Computing for Investigations of Electronic Transitions in Phenylsulfonyl-carbazole TADF Emitters. *npj Quant. Inf.* **7**, 70 (2021).
28. O'Brien, T. E. et al. Purification-based Quantum Error Mitigation of Pair-Correlated Electron Simulations. Preprint at https://doi.org/10.48550/arXiv.2210.10799 (2022).
29. Limacher, P. A. et al. The Influence of Orbital Rotation on the Energy of Closed-Shell Wavefunctions. *Mol. Phys.* **112**, 853–862 (2014).
30. Henderson, T. M., Bulik, I. W. & Scuseria, G. E. Pair Extended Coupled Cluster Doubles. *J. Chem. Phys.* **142**, 214116 (2015).
31. Zhao, L. & Neuscamman, E. Amplitude Determinant Coupled Cluster with Pairwise Doubles. *J. Chem. Theory Comput.* **12**, 5841–5850 (2016).
32. Sokolov, I. O. et al. Quantum Orbital-Optimized Unitary Coupled Cluster Methods in the Strongly Correlated Regime: Can Quantum Algorithms Outperform Their Classical Equivalents? *J. Chem. Phys.* **152**, 124107 (2020).
33. Sun, Q. et al. Pyscf: the python-based simulations of chemistry framework. *Wiley Interdiscip. Rev. Comput. Mol. Sci.* **8**, e1340 (2018).
34. Kawashima, Y. et al. Optimizing Electronic Structure Simulations on a Trapped-Ion Quantum Computer using Problem Decomposition. *Commun. Phys.* **4**, 245 (2021).
35. Johri, S. et al. Nearest Centroid Classification on a Trapped Ion Quantum Computer. *npj Quant. Inf.* **7**, 122 (2021).
36. Rudolph, M. S. et al. Generation of High-Resolution Handwritten Digits with an Ion-Trap Quantum Computer. *Phys. Rev. X* **12**, 031010 (2022).
37. Zhu, E. Y. et al. Generative Quantum Learning of Joint Probability Distribution Functions. *Phys. Rev. Res.* **4**, 043092 (2022).
38. Giurgica-Tiron, T. et al. Low-depth Amplitude Estimation on a Trapped-Ion Quantum Computer. *Phys. Rev. Res.* **4**, 033034 (2022).
39. Aspuru-Guzik, A., Dutoi, A. D., Love, P. J. & Head-Gordon, M. Simulated Quantum Computation of Molecular Energies. *Science* **309**, 1704–1707 (2005).
40. Lanyon, B. P. et al. Towards Quantum Chemistry on a Quantum Computer. *Nat. Chem.* **2**, 106–111 (2010).
41. Babbush, R. et al. Encoding Electronic Spectra in Quantum Circuits with Linear T Complexity. *Phys. Rev. X* **8**, 041015 (2018).
42. Low, G. H. & Chuang, I. L. Hamiltonian Simulation by Qubitization. *Quantum* **3**, 163 (2019).
43. Lee, J. et al. Even More Efficient Quantum Computations of Chemistry Through Tensor Hypercontraction. *PRX Quant.* **2**, 030305 (2021).
44. Colless, J. I. et al. Computation of Molecular Spectra on a Quantum Processor with an Error-Resilient Algorithm. *Phys. Rev. X* **8**, 011021 (2018).
45. Takeshita, T. et al. Increasing the Representation Accuracy of Quantum Simulations of Chemistry without Extra Quantum Resources. *Phys. Rev. X* **10**, 011004 (2020).
46. McArdle, S., Yuan, X. & Benjamin, S. Error-Mitigated Digital Quantum Simulation. *Phys. Rev. Lett.* **122**, 180501 (2019).
47. Hashim, A. et al. Randomized Compiling for Scalable Quantum Computing on a Noisy Superconducting Quantum Processor. *Phys. Rev. X* **11**, 041039 (2021).
48. Urbanek, M. et al. Mitigating Depolarizing Noise on Quantum Computers with Noise-Estimation Circuits. *Phys. Rev. Lett.* **127**, 270502 (2021).
49. Lubinski, T. et al. Application-Oriented Performance Benchmarks for Quantum Computing. *IEEE Trans. Quant. Eng.* **4**, 1–32 (2023).
50. Vatan, F. & Williams, C. Optimal Quantum Circuits for General Two-Qubit Gates. *Phys. Rev. A* **69**, 032315 (2004).
51. Elfving, V. E., Millaruelo, M., Gámez, J. A. & Gogolin, C. Simulating Quantum Chemistry in the Seniority-Zero Space on Qubit-based Quantum Computers. *Phys. Rev. A* **103**, 032605 (2021).
52. Khan, I. et al. Chemically Aware Unitary Coupled Cluster with ab initio Calculations on System Model H1: A Refrigerant Chemicals Application. *J. Comp. Phys.* **158**, 214114 (2023).

53. Kirsopp, J. J. et al. Quantum Computational Quantification of Protein–Ligand Interactions. *Int. J. Quant. Chem.* **122**, e26975 (2022).
54. Yamamoto, K., Manrique, D. Z., Khan, I. T., Sawada, H. & Ramo, D. M. Quantum Hardware Calculations of Periodic Systems with Partition-Measurement Symmetry Verification: Simplified Models of Hydrogen Chain and Iron Crystals. *Phys. Rev. Res.* **4**, 033110 (2022).
55. Motta, M. et al. Quantum Chemistry Simulation of Ground-and Excited-State Properties of the Sulfonium Cation on a Superconducting Quantum Processor. *Chem. Sci.* **14**, 2915 (2023).
56. Eddins, A. et al. Doubling the Size of Quantum Simulators by Entanglement Forging. *PRX Quant.* **3**, 010309 (2022).
57. Gao, Q. et al. Computational Investigations of the Lithium Superoxide Dimer Rearrangement on Noisy Quantum Devices. *J. Phys. Chem. A* **125**, 1827–1836 (2021).

AUTHOR CONTRIBUTIONS
L.Z., K.S., W.K., and J.K. conceived of the project. L.Z. and K.S. designed, implemented, and evaluated the algorithms. Experimental data were collected and analyzed by K.W., J.N., and L.Z.; All authors contributed to drafting and editing the paper.

COMPETING INTERESTS
The authors declare no competing interests.

ADDITIONAL INFORMATION
Supplementary information The online version contains supplementary material available at https://doi.org/10.1038/s41534-023-00730-8.

Correspondence and requests for materials should be addressed to Luning Zhao or Kyujin Shin.

Reprints and permission information is available at http://www.nature.com/reprints

Publisher's note Springer Nature remains neutral with regard to jurisdictional claims in published maps and institutional affiliations.